# Splicing variation of Long-IRBIT determines the target selectivity of IRBIT family proteins

Katsuhiro Kawaai[a], Hideaki Ando[a], Nobuhiko Satoh[b], Hideomi Yamada[b], Naoko Ogawa[a], Matsumi Hirose[a], Akihiro Mizutani[c], Benjamin Bonneau[a], George Seki[b], and Katsuhiko Mikoshiba[a,1]

[a]Laboratory for Developmental Neurobiology, Brain Science Institute, RIKEN, Wako, Saitama 351-0198, Japan; [b]Department of Internal Medicine, University of Tokyo, Bunkyo-ku, Tokyo 113-0033, Japan; and [c]Department of Pharmacotherapeutics, Showa Pharmaceutical University, Machida, Tokyo 194-8543, Japan

Edited by Solomon H. Snyder, The Johns Hopkins University School of Medicine, Baltimore, MD, and approved February 28, 2017 (received for review November 8, 2016)

**IRBIT [inositol 1,4,5-trisphosphate receptor ($IP_3R$) binding protein released with inositol 1,4,5-trisphosphate ($IP_3$)] is a multifunctional protein that regulates several target molecules such as ion channels, transporters, polyadenylation complex, and kinases. Through its interaction with multiple targets, IRBIT contributes to calcium signaling, electrolyte transport, mRNA processing, cell cycle, and neuronal function. However, the regulatory mechanism of IRBIT binding to particular targets is poorly understood. Long-IRBIT is an IRBIT homolog with high homology to IRBIT, except for a unique N-terminal appendage. Long-IRBIT splice variants have different N-terminal sequences and a common C-terminal region, which is involved in multimerization of IRBIT and Long-IRBIT. In this study, we characterized IRBIT and Long-IRBIT splice variants (IRBIT family). We determined that the IRBIT family exhibits different mRNA expression patterns in various tissues. The IRBIT family formed homo- and heteromultimers. In addition, N-terminal splicing of Long-IRBIT changed the protein stability and selectivity to target molecules. These results suggest that N-terminal diversity of the IRBIT family and various combinations of multimer formation contribute to the functional diversity of the IRBIT family.**

IRBIT | Long-IRBIT | splice variant | protein stability | protein–protein interaction

It was recently proposed that protein–protein interaction networks are scale-free, in that most of the proteins bind to one or two targets but relatively fewer "hub proteins" interact with 10 or more targets (1). The scale-free property of protein–protein interactions provides the advantages of high connectivity and robustness for physiological basis. However, dysfunction of hub proteins can lead to the impairment of whole signaling networks (2). Therefore, it is important to understand the regulatory mechanisms of hub proteins. IRBIT [inositol 1,4,5-trisphosphate receptor ($IP_3R$) binding protein released with inositol 1,4,5-trisphosphate ($IP_3$)] is a multifunctional protein that interacts with diverse target molecules, and therefore is assumed to function as a hub protein. IRBIT was originally identified as a molecule that interacts with the intracellular calcium channel, $IP_3R$. IRBIT binds to the $IP_3$ binding domain of $IP_3R$ and suppresses its activation (3). However, IRBIT binds to multiple ion channels and transporters, including sodium bicarbonate cotransporter 1 (NBCe1) (4–7), cystic fibrosis transmembrane conductance regulator (CFTR) (6–8), solute carrier family 26 member 6 (Slc26a6) (7, 8), and sodium hydrogen exchanger 3 (NHE3) (9–12). It also contributes to intracellular pH regulation and fluid secretion (6–8). In addition, IRBIT binds to cleavage and polyadenylation-specific factor subunit (Fip1) and modulates the polyadenylation state of specific mRNA (13). It was also reported that IRBIT regulates ribonucleotide reductase and contributes to cell cycle progression (14). Moreover, IRBIT forms signaling complexes with phosphatidylinositol phosphate kinases (15). It was also reported that IRBIT contributes in apoptosis regulation (16). In the central nervous system, IRBIT binds to calcium calmodulin-dependent kinase II-α (CaMKIIα) and contributes to catecholamine homeostasis (17). Accordingly, IRBIT contributes to calcium signaling, electrolyte transport, mRNA processing, cell cycle, apoptosis, and the regulation of catecholamine homeostasis through its interaction with multiple targets. However, how IRBIT selectively binds and regulates appropriate target molecules in certain conditions and regulates various intracellular signaling pathways is poorly understood.

We previously reported the discovery of the IRBIT homolog, Long-IRBIT (18). Although Long-IRBIT has overall high homology with IRBIT, except for a unique N-terminal appendage, it has low binding affinity to $IP_3R$. Recently, it was reported that there were splice variants of Long-IRBIT in the human transcripts database (variant 3: NM_001130722, variant 4: NM_001130723). These splice variants have different N-terminal sequences and a common C-terminal region, which is involved in multimerization of IRBIT and Long-IRBIT. Therefore, it is possible that splicing variants have different molecular properties and form a multimer with IRBIT to achieve functional diversity. In this study, we cloned mouse homologs of Long-IRBIT splice variants and characterized the expression pattern, protein stability, and regulation of several IRBIT target molecules. These results demonstrate that the N-terminal diversity of the IRBIT family and various combinations of multimer formations contribute to the functional diversity of the IRBIT family.

## Results

We first characterized Long-IRBIT (variant 2: NM_001130720) in 2009 (18). Novel splice variants of Long-IRBIT have been deposited in the human transcripts database (variant 1: NM_015328,

### Significance

**IRBIT (inositol 1,4,5-trisphosphate receptor binding protein released with inositol 1,4,5-trisphosphate) contributes to calcium signaling, electrolyte transport, mRNA processing, genomic integrity, and catecholamine homeostasis through its interaction with multiple targets. However, how IRBIT selectively binds and regulates appropriate target molecules in a certain condition is poorly understood. In this study, we found that N-terminal variation of Long-IRBIT by splicing affected protein stability and target selectivity. In addition, IRBIT and Long-IRBIT splice variants formed homo- and heteromultimers. N-terminal variation of IRBIT family members mediates the regulation of multiple signaling pathways.**

Author contributions: K.K., H.A., A.M., B.B., G.S., and K.M. designed research; K.K., N.S., H.Y., N.O., and M.H. performed research; K.K., H.A., N.S., H.Y., N.O., and M.H. analyzed data; and K.K., H.A., A.M., B.B., G.S., and K.M. wrote the paper.

The authors declare no conflict of interest.

This article is a PNAS Direct Submission.

Data deposition: The sequence reported in this paper has been deposited in the GenBank database (accession no. AB470072.1).

[1]To whom correspondence should be addressed. Email: mikosiba@brain.riken.jp.

This article contains supporting information online at www.pnas.org/lookup/suppl/doi:10.1073/pnas.1618514114/-/DCSupplemental.

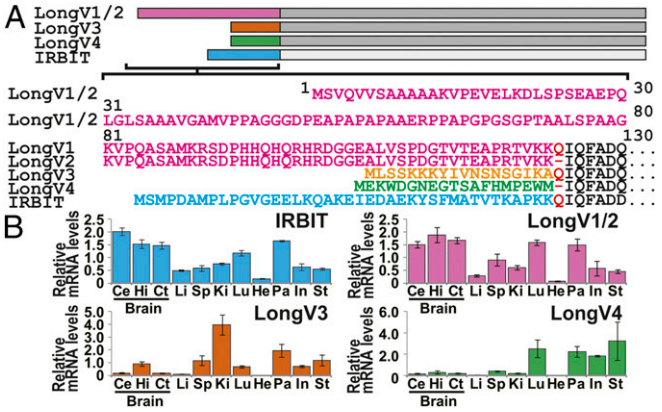


**Fig. 1.** Tissue distribution of IRBIT family. (*A*) Schematic illustration of IRBIT family and N-terminal amino acid sequence. (*B*) Tissue distribution of IRBIT family mRNA expression. $n = 3$. Ce, cerebellum; Ct, cerebral cortex; He, heart; Hi, hippocampus; In, intestine; Ki, kidney; Li, liver; Lu, lung; Sp, spleen; St, stomach; Pa, pancreas.

variant 3: NM_001130722, variant 4: NM_001130723) (Fig. S1*A*). Variant 1 is highly similar to the previously characterized variant 2. We first cloned the mouse homologs of Long-IRBIT splice variant 3 (LongV3) and variant 4 (LongV4) from the mouse forebrain using specific primers (Fig. 1*A* and Table S1). We also obtained three different transcripts of LongV3 (3a, 3b, and 3c in Fig. S1 *B* and *C*), and characterized LongV3a, which is deposited in GenBank (NM_001171001). We previously reported that the N-terminal region of IRBIT is intrinsically highly disordered (15). Therefore, we evaluated the structural disorder of Long-IRBIT splice variants using an in silico prediction program (PONDR-FIT) (19). The N-terminal region of Long-IRBIT splice variants was highly disordered, similar to IRBIT (Fig. S1*D*). Therefore, the N terminus of IRBIT family proteins (IRBIT and Long-IRBIT splice variants) belongs to the intrinsically disordered protein regions.

We analyzed the mRNA expression of IRBIT and Long-IRBIT splice variants in adult mouse organs by quantitative PCR analysis using specific primers (Table S1). It was technically difficult to distinguish between Long-IRBIT splice variants 1 and 2 (LongV1 and LongV2), because the difference between LongV1 and LongV2 is only 1 aa at the splice site (Fig. 1*A*). IRBIT and LongV1/2 were expressed in various tissues and highly expressed in the pancreas and brain (Fig. 1*B*). LongV3 was mainly expressed in the kidney and LongV4 was expressed in the lung, pancreas, small intestine, and stomach. We generated a specific antibody (Ab) against LongV4. The anti-LongV4 Ab specifically recognized LongV4 of 60 kDa, but not IRBIT, LongV2, or LongV3 (Fig. S2*A*). We also confirmed the specificity of IRBIT Ab (20), LongV1/2 Ab (18), and pan-IRBIT Ab (18). The anti-IRBIT and anti-LongV1/2 Abs specifically recognized IRBIT and LongV2, respectively, whereas the anti–pan-IRBIT Ab recognized IRBIT, LongV2, LongV3, and LongV4 (Fig. S2*B*). Western blot analysis of anti-LongV4 revealed that it is highly expressed in the stomach and poorly expressed in the pancreas (Fig. S2*C*). Immunostaining using anti-LongV4 Ab showed that the strong immunosignal was observed in the stomach, compared with the brain (Fig. S2*D*). In the stomach, LongV4 was expressed in gastric parietal cells, which were stained with the proton pump HKATPase (Fig. S2*E*). LongV4 was expressed near the basal membrane, whereas HKATPase staining was observed around the intracellular canaliculi. These results demonstrate tissue-specific expression of Long-IRBIT splice variants. Additionally, we found that gene expression of Long-IRBIT splice variants was regulated during postnatal brain development and neuronal maturation (Fig. S2 *F*–*M*).

Because we previously reported that Long-IRBIT (LongV2) interacts with IRBIT through the C-terminal region (18), we conducted a coimmunoprecipitation (co-IP) assay in COS-7 cells expressing HA- or Flag-tagged IRBIT and Long-IRBIT splice variants. IRBIT and Long-IRBIT splicing variants were coimmunoprecipitated with each other (Fig. 2 *A* and *B*). In addition, we found that multimer formation of the IRBIT family depends on the protein synthesis and folding process (Fig. S3*A*; details described in *SI Discussion*). We also performed a co-IP assay in stomach lysates using anti-IRBIT, anti-LongV1/2, or anti-LongV4 antibodies. Endogenous IRBIT, LongV1/2, and LongV4 were coimmunoprecipitated (Fig. 2*C*). Quantification of signal intensities of IRBIT, LongV1/2, and LongV4 detected by anti–pan-IRBIT Ab suggest that LongV4 is the dominant isoform in stomach and forms both homo- and heteromultimer, whereas IRBIT and LongV1/2 form predominantly heteromultimer with LongV4 (Fig. 2*D*; detailed prediction described in *SI Discussion*). Immunostaining of the stomach showed that IRBIT, LongV1/2, and LongV4 were expressed in gastric parietal cells (Fig. 2*E*). These data suggested that IRBIT family proteins form heteromultimers in stomach parietal cells.

We previously reported that Long-IRBIT (LongV2) has a lower binding affinity than IRBIT for $IP_3R1$, although LongV2 completely conserved the critical amino acids of IRBIT required for the interaction with $IP_3R1$ (18). Binding analysis using deletion mutants of LongV2 revealed that low affinity to $IP_3R1$ is attributable to an inhibitory effect of the LongV2-specific N-terminal region (18). Therefore, it is possible that N-terminal splicing determines the binding affinity of the IRBIT family to target molecules. We performed a binding assay using the IRBIT family proteins and several representative target molecules (NBCe1-C, NHE3, Fip1L, CaMKIIα, and $IP_3R1$). We previously reported that IRBIT binds to NBCe1-B (pancreatic type NBCe1) and regulates NBCe1-B activity (4). Recently, we cloned a brain type NBCe1 (NBCe1-C, GenBank accession no. AB470072.1), which has an IRBIT binding domain in common with NBCe-1B. Therefore, we investigated the

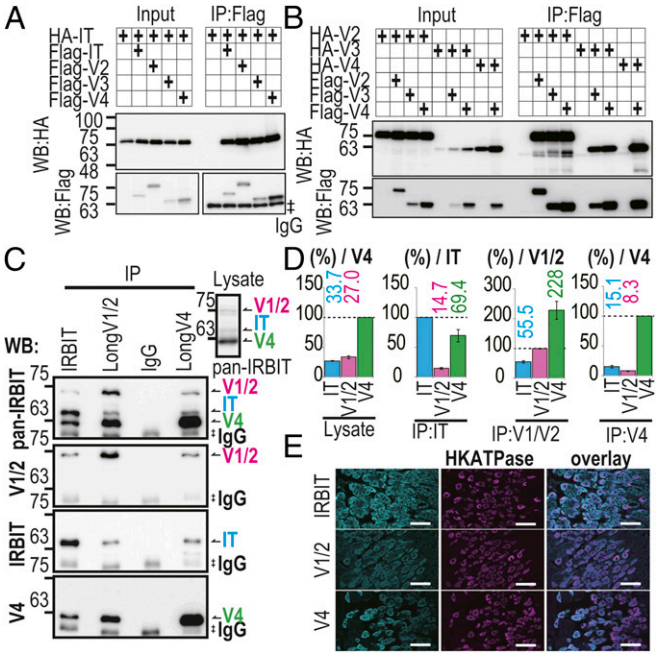


**Fig. 2.** Multimer formation of IRBIT family. IT, IRBIT; V1/2, LongV1/2; V3, LongV3; V4, LongV4. (*A*) Co-IP of HA-IRBIT and Flag-IRBIT family. ‡IgG bands for IP. (*B*) Co-IP of HA–Long-IRBITs and Flag–Long-IRBITs. (*C*) Co-IP assay of IRBIT, LongV1/2, and LongV4 from stomach lysates. ‡IgG bands for IP. (*D*) Quantification of IRBIT, LongV1/2, and LongV4 by pan-IRBIT Ab in *C*. (*E*) Adult mouse stomach section was stained with anti-IRBIT, anti-LongV1/2, or anti-LongV4 Abs (cyan), and anti-HKATPase Ab (magenta). (Scale bars, 50 μm.)

interaction between NBCe1-C and the IRBIT family. COS-7 cell lysates expressing and the HA-IRBIT family and target molecule (GFP–NBCe1-C, NHE3-GFP, or Fip1L-myc) were immunoprecipitated using an anti-HA Ab. GFP–NBCe1-C bound strongly to HA-IRBIT and HA-LongV3 and bound weakly to HA-LongV2 and HA-LongV4 (Fig. 3 *A* and *F*). GFP-NHE3 bound strongly to HA-LongV2 and HA-LongV3 and bound weakly to HA-IRBIT and HA-LongV4 (Fig. 3 *B* and *F*). Fip1L-myc was equally precipitated with HA-IRBIT, HA-LongV3, and HA-LongV4, whereas HA-LongV2 bound weakly to Fip1L-myc (Fig. 3 *C* and *F*). COS-7 cell lysates expressing HA-CaMKIIα and Flag-IRBIT family proteins were immunoprecipitated using an anti-Flag Ab. HA-CaMKIIα was equally precipitated with HA-IRBIT, HA-LongV2, and HA-LongV4, whereas HA-LongV3 bound strongly to HA-CaMKIIα (Fig. 3 *D* and *F*). Finally, COS-7 cell lysates expressing HA-IRBIT family proteins were applied to the purified GST-tagged N-terminal region of $IP_3R1$ (GST-EL) (18). HA-IRBIT and HA-LongV4 bound strongly to $IP_3R1$ (Fig. 3 *E* and *F*). HA-LongV2 and HA-LongV3 bound weakly to $IP_3R1$. The radar chart of relative binding affinities for each target molecule indicates that IRBIT family proteins have different binding properties (Fig. 3*G*). We also performed binding assay using the N-terminal deletion mutant of Long-IRBIT, which strongly bound to target molecules (NBCe1-C, NHE3, Fip1L, and $IP_3R1$), except with CaMKIIα (Fig. S3 *C–H*; details described in *SI Discussion*). From these results, we concluded that N-terminal splicing determines the binding affinity of the IRBIT family to target molecules.

We observed that the expression level of LongV3 was lower than other variants in transfected COS-7 cells. Therefore, we investigated the effect of the proteasome inhibitor, MG-132 (10 μM), or protein biosynthesis inhibitor, cycloheximide (CHX, 50 μg/mL) on the expression of HA-tagged IRBIT and Long-IRBIT splice variants. LongV3 protein markedly accumulated with MG-132 (Fig. 3 *H* and *I*). Conversely, the protein degradation rate of LongV3 after CHX treatment was significantly higher than IRBIT, LongV2, and LongV4 (Fig. 3 *J* and *K*). These data suggest that N-terminal splicing of Long-IRBIT determines protein stability. We also examined the effect of the N-terminal tag, N-terminal deletion of specific sequences, coexpression of target molecules, and the point mutant disturbing the interaction with target molecules (3, 4, 13) on MG-132 treatment (Fig. S4; details described in *SI Discussion*). From these results, we concluded that N-terminal splicing of Long-IRBIT determines protein stability.

Because IRBIT and LongV4 strongly bound to $IP_3R1$ compared with LongV2 and LongV3 (Fig. 3 *E* and *F*), we investigated the effect of IRBIT family expression on the channel activity of $IP_3R$. Because endogenous IRBIT significantly inhibited the channel activity of $IP_3R$ (Fig. S5*A*) and masked the effect of IRBIT overexpression on $IP_3R$ (3), we transfected the mRFP-P2A-IRBIT family into IRBIT knockout (KO) mouse embryonic fibroblast (MEF) cells (15). The expression levels of IRBIT family were confirmed (Fig. S5 *B–H*). Transfected MEF cells were loaded with the calcium indicator, Fura-2, and stimulated using 1, 3, and 5 μM ATP. We found that the peak amplitude of $Ca^{2+}$ transients was significantly inhibited by the expression of IRBIT and LongV4 compared with mRFP-P2A, whereas the expression of LongV2 and LongV3 did not affect $Ca^{2+}$ transients (Fig. 4 *A–F* and Fig. S5*I*). Consistent results were obtained in a supplemental experiment of MEF cells in an extracellular $Ca^{2+}$-free condition and of IRBIT KO HeLa cells (16) using histamine stimulation or caged-$IP_3$ photo-uncaging (Fig. S5 *J–N*). These results suggest that LongV4 suppresses $IP_3R$ activity, as observed with IRBIT (3). We next investigated the effect of IRBIT family expression on CaMKIIα activation using a FRET-based CaMKIIα activity probe (Camuiα). We performed simultaneous imaging of $Ca^{2+}$-ionophore (4-Bromo-A23187, BrA) -induced $Ca^{2+}$ and Camuiα FRET changes in IRBIT KO MEF cells (Fig. 4 *G–L*). Consistent with a previous study (17), the expression of IRBIT significantly inhibited the BrA-induced Camuiα FRET change, but did not affect the $Ca^{2+}$ change. In addition, the expression of Long-IRBIT splice variants also significantly inhibited the BrA-induced Camuiα FRET change, but did not affect the $Ca^{2+}$ change. Notably, consistent with the strong binding affinity of LongV3 to CaMKIIα (Fig. 3 *D* and *F*), LongV3 strongly inhibits CaMKIIα activity. We concluded that all of the IRBIT family regulated CaMKIIα activity.

We next investigated the effect of IRBIT family expression on NHE3-dependent pH changes. IRBIT KO MEF cells were transfected with NHE3/mRFP, and seBFP-P2A-IRBIT family and $Na^+$-dependent intracellular pH change was measured using the pH indicator 2′,7′-bis-(2-carboxyethyl)-5-(and-6)-carboxyfluorescein (BCECF). He et al. previously showed that IRBIT contributed to insulin-induced or angiotensin II-induced activation of pH recovery through NHE3 transport in opossum kidney proximal tubule (OKP) cells (9–11). In addition, Tran et al. showed that IRBIT knockdown inhibited NHE3-dependent pH recovery from cell acidification in human submandibular gland cells (12). Unexpectedly, IRBIT expression significantly inhibited $Na^+$-dependent intracellular pH change in NHE3 expressed IRBIT KO MEF cells (Fig. 5 *A* and *B*). However, LongV3 significantly activated NHE3 activity.

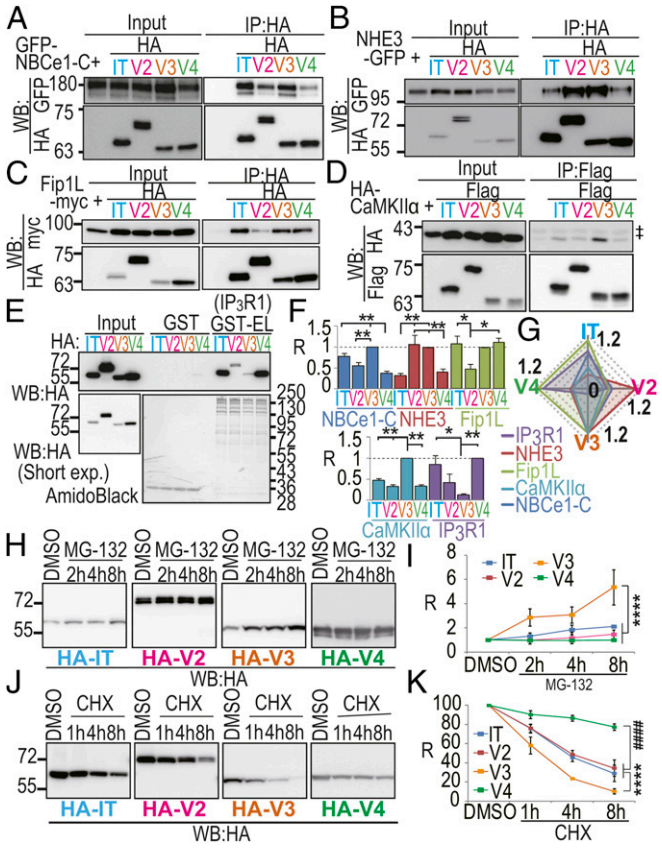


**Fig. 3.** Co-IP assay for IRBIT family and target molecules and protein stability of IRBIT family. IT, IRBIT; V2, LongV2; V3, LongV3; and V4, LongV4. (*A*) Co-IP of HA-IRBIT family and GFP–NBCe1-C, $n = 4$. (*B*) Co-IP of HA-IRBIT family and NHE3-GFP, $n = 4$. (*C*) Co-IP of HA-IRBIT family and Fip1L-myc, $n = 4$. (*D*) Co-IP of Flag-IRBIT family and HA-CaMKIIα. ‡IgG for IP $n = 3$. (*E*) Pull-down assay of HA-IRBIT family and GST-tagged N-terminal region of $IP_3R1$ (GST-EL), $n = 4$. (*F*) Quantification of binding assay in *A–E*. Data were normalized by LongV3 for *A–D* and normalized by LongV4 for *E*. R, Relative value. $^*P < 0.05$, $^{**}P < 0.01$. (*G*) Radar chart of each target molecules for IRBIT family. (*H*) Transfected COS-7 cells with HA-IRBIT family were treated with MG-132 (10 μM) or DMSO. (*I*) Quantitative analysis of HA-IRBIT family in *H*, $n = 3$. $^{****}P < 0.0001$. (*J*) Transfected COS-7 cells with HA-IRBIT family were treated with CHX (50 μg/mL) or DMSO. (*K*) Quantitative analysis of HA-IRBIT family in *J*, $n = 3$. $^{****}P < 0.0001$, $^{\#\#\#\#}P < 0.0001$.

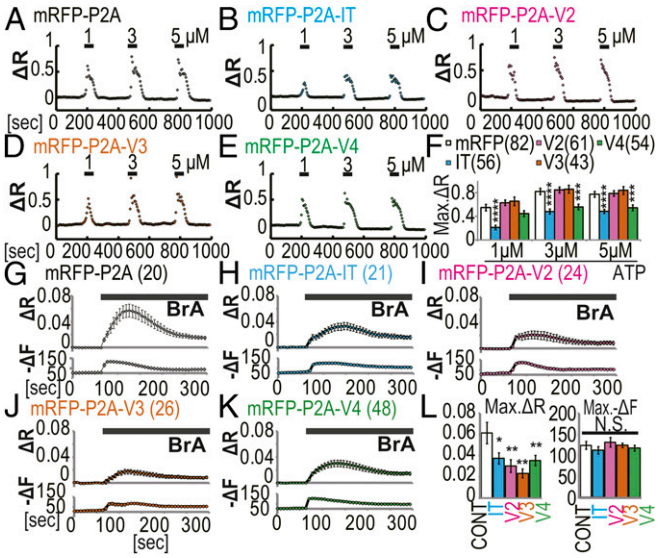

**Fig. 4.** IRBIT family regulated ATP-induced $Ca^{2+}$ release activity and CaMKIIα activation. IT, IRBIT; V2, LongV2; V3, LongV3; V4, LongV4. (*A–E*) Representative $Ca^{2+}$ imaging of transfected IRBIT KO MEF cells. (*F*) Quantitation of $Ca^{2+}$ peak amplitude (Max. ΔR) in transfected IRBIT KO MEF cells. ***$P < 0.001$, ****$P < 0.0001$. (*G–K*) Simultaneously imaging of FRET and $Ca^{2+}$ change in transfected IRBIT KO MEF cells. (*Upper*) Average FRET changes (ΔR) are shown. (*Lower*) Average $Ca^{2+}$ responses (−ΔF) are shown. BrA: 2.5 μM. (*L*) Quantitation of FRET amplitude (Max. ΔR) and $Ca^{2+}$ peak amplitude (Max. −ΔF). *$P < 0.05$, **$P < 0.01$, N.S., no significance.

LongV2 and LongV4 slightly inhibited NHE3 activity, but no significant difference was observed. To eliminate the effect of endogenous NHE1 activity, we performed the same experiment in the presence of 30 μM amiloride (AML), which strongly inhibits NHE1 and partially inhibits NHE3 (21). In the presence of 30 μM AML, we observed gradual acidification in IRBIT KO MEF cells expressing mRFP alone (Fig. S6*A*). Expression of NHE3/mRFP significantly inhibited gradual acidification in IRBIT KO MEF cells (Fig. S6 *A* and *B*). Consistent with results in the absence of AML, the expression of LongV3 activated NHE3 activity in the presence of 30 μM AML (Fig. S6 *C* and *D*). However, IRBIT and LongV2 inhibited NHE3 activity and LongV4 had no effect. From these results, we concluded that IRBIT inhibits NHE3 activity and LongV3 promotes NHE3 activity, at least in MEF cells.

We examined the effect of IRBIT family protein expression on NBCe1-C activity. Because endogenous IRBIT significantly activated the NBCe1-C activity (Fig. S6*E*), IRBIT KO MEF cells were transfected with the expression vector NBCe1-C/mRFP and seBFP-P2A-IRBIT family and $Na^+$-dependent intracellular pH changes were measured using BCECF. Consistent with the binding affinity (Fig. 3*A*), IRBIT and LongV3 significantly activated NBCe1-C, whereas LongV2 and LongV4 had no effect (Fig. 5 *C* and *D*). To further confirm the activation of NBCe1 by IRBIT and LongV3, we performed an electrophysiological analysis in *Xenopus* oocytes. Oocytes were injected with NBCe1-B and seBFP-P2A, seBFP-P2A-IRBIT, or seBFP-P2A-LongV3 cRNA. Expression and cleavage of seBFP at the P2A site of IRBIT and LongV3 were verified by Western blotting using pan-IRBIT and GFP Abs (Fig. S6*F*). Injected oocytes were then perfused with an $HCO_3^-/CO_2$ solution, and the negative charge influx (current) was measured at a holding potential of −25 mV. Consistent with the pH imaging data, IRBIT and LongV3 significantly activated NBCe1-B compared with seBFP-P2A alone (Fig. 5*E*). We analyzed the current–voltage (*I–V*) relationship by applying step pulses between $V_m = -120$ and 80 mV. The expression of IRBIT and LongV3 markedly activated the NBCe1-B current over the entire voltage range (Fig. 5*F*).

Although NBCe1-C bound weakly to LongV2 and LongV4 (Fig. 3 *A* and *F*), both did not activate NBCe1-C activity (Fig. 5 *C* and *D*). To evaluate whether the N-terminal of LongV2 disturbed the activation of NBCe1, we constructed N-terminal deletion mutants of LongV2 and performed a binding assay as well as measured NBCe1-B activity. N-terminal deletion sites are illustrated in Fig. 6*A* and Fig. S6*G*. Cell lysates of COS-7 cells expressing HA-LongV2 and deletion mutants were applied to the purified MBP tagged N-terminal region of NBCe1-B (MBP–NBCe1-B/N1) (4). Deletion mutants from Δ20 to Δ157 bound to NBCe1-B similar to full-length LongV2, whereas mutants deleted for more than 174 N-terminal amino acids no longer bound to NBCe1-B (Fig. 6*B*). Consistent results were obtained by co-IP assay using GFP–NBCe1-B and HA-tagged deletion mutants of LongV2 (Fig. 6*C*). We performed an electrophysiological analysis of NBCe1-B with LongV2 deletion mutants in *Xenopus* oocytes. IRBIT activated NBCe1-B, whereas the full-length HA-LongV2 did not (Fig. 6*D*). Interestingly, the LongV2 mutant with deleted N-terminal 139 and 157 aa (Δ139 and Δ157) significantly activated NBCe1-B compared with full-length LongV2. However, other deletion mutants were unable to activate NBCe1-B. These results indicate that N-terminal 138 aa of LongV2 and 36 aa of LongV4 disturbed their ability to activate NBCe1-B.

We next investigated the effects of overexpression of Long-IRBIT splicing variants on $IP_3R$ activity in stomach parietal cells, in which LongV2 and LongV4 were natively expressed (Fig. 2 *C–E*). Overexpression of LongV2 or LongV4 was clearly observed in $mRFP^+$ cells (Fig. 7*A*). Transfected gastric glands were loaded with Fura-2, and stimulated using 100 μM carbachol (CCh) in extracellular $Ca^{2+}$-free condition. Overexpression of LongV4 significantly inhibited CCh-induced $Ca^{2+}$ release, compared with control cells expressing mRFP-P2A, but overexpression of LongV2 did not affect it (Fig. 7 *B* and *C*). Therefore, selectively, LongV4 regulated $IP_3R$ activity in stomach gastric glands. Finally, we examined the effect of LongV2 coexpression with IRBIT to investigate whether the heteromultimer formation of IRBIT family affects target selectivity. Because heteromultimer formation of IRBIT and Long-IRBIT splicing variants was dependent

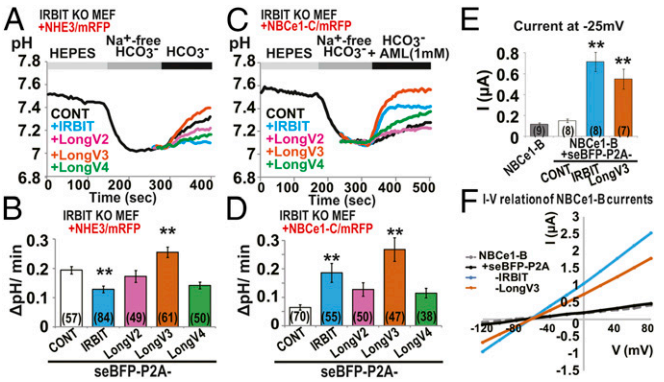

**Fig. 5.** IRBIT family regulated NHE3 and NBCe1 activity. (*A*) Representative pH imaging of transfected IRBIT KO MEF cells with NHE3/mRFP. (*B*) Quantitation of intracellular pH change (ΔpH/min) after switching from $Na^+$-free to 144 mM $Na^+/HCO_3^-$ buffer. The total cell numbers were indicated in each graph. **$P < 0.01$. (*C*) Representative pH imaging of transfected IRBIT KO MEF cells with NBCe1-C/mRFP. (*D*) Quantitation of intracellular pH change (ΔpH/min) after switching from $Na^+$-free to 144 mM $Na^+$ $HCO_3^-$ buffer with NHE1 inhibitor, AML (1 mM). **$P < 0.01$. (*E*) NBCe1-B–mediated currents in *Xenopus* oocyte. Influxes of anion charges were measured at a holding potential of −25 mV. **$P < 0.01$. (*F*) Current–voltage (*I–V*) relationship of NBCe1-B currents in oocytes. Step pulses between $V_m = -120$ and 80 mV were applied.

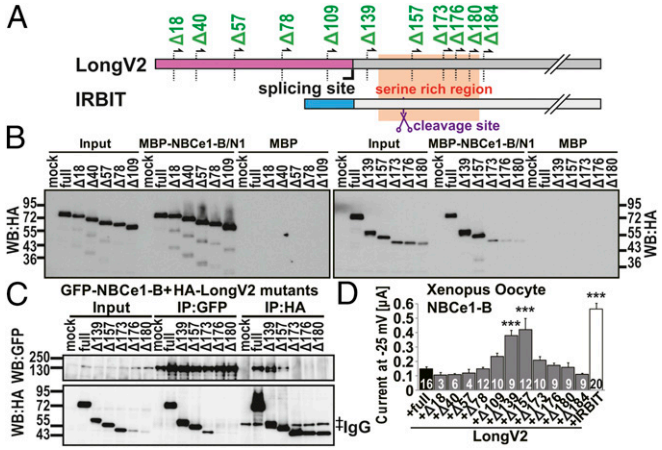


**Fig. 6.** N-terminal of LongV2 disturbed the activation of NBCe1-B. (*A*) Schematic illustration of N-terminal deletion mutants for binding assay and electrophysiological analysis. (*B*) Pull-down assay of HA-LongV2 deletion mutants and MBP-tagged N-terminal region of NBCe1-B. (*C*) Co-IP of GFP–NBCe1-B and HA-LongV2 deletion mutants. ‡IgG bands for IP. (*D*) NBCe1-B–mediated currents at a holding potential of −25 mV in *Xenopus* oocyte injected NBCe1-B cRNA with full-length LongV2 (full), various LongV2 deletion mutants, or IRBIT. ***$P < 0.001$ compared with full-length LongV2. The total cell numbers were indicated in each graph.

on the protein synthesis and folding process (Fig. S3*A*), IRBIT KO MEF cells were cotransfected with the expression vector IRBIT/eGFP and mRFP-P2A or mRFP-P2A-LongV2, and ATP-induced calcium change was measured by Fura-2. The inhibition of $IP_3R$ activity by IRBIT was attenuated by LongV2 coexpression (Fig. 7*D*). In addition, we performed electrophysiological analysis in *Xenopus* oocytes to investigate the effect of LongV2 coexpression on the activation of NBCe1 by IRBIT. IRBIT significantly activated NBCe1-B compared with NBCe1-B alone, whereas LongV2 did not activate NBCe1-B (Fig. 7*E*). Coexpression of LongV2 with IRBIT significantly blocked NBCe1-B activation by IRBIT. From these results, we concluded that the IRBIT family forms a heteromultimer and determines target selectivity.

## Discussion

We investigated the characteristic properties of Long-IRBIT splice variants. We identified the expression of LongV4, LongV3b, and LongV3c as transcripts in the mouse brain cDNA (Fig. 1*A* and Fig. S1 *A*–*C*). In addition, we showed that: (*i*) different expression patterns of Long-IRBIT splice variants exist in various tissues and LongV4 is highly expressed in the basal membrane of stomach parietal cells; (*ii*) expression of Long-IRBIT splice variants drastically changed from LongV3/4 to LongV1/2 during mouse brain development and LongV1/2 expression increased during synaptogenesis of hippocampal neuronal culture; (*iii*) IRBIT and Long-IRBIT splice variants form homo- and heteromultimers in the stomach lysate; (*iv*) N-terminal splicing of Long-IRBIT changes protein stability; and (*v*) N-terminal splicing determines the binding affinity of IRBIT family proteins to target molecules and their selectivity to target pathways (intracellular calcium release, CaMKIIα activation, pH regulation, and so forth).

In previous studies, IRBIT contributed to insulin-induced or angiotensin II-induced activation of pH recovery through NHE3 transport in OKP cells (9–11). In addition, IRBIT knockdown inhibited NHE3-dependent pH recovery from cell acidification in human submandibular gland cells (12). However, IRBIT expression significantly inhibited $Na^+$-dependent intracellular pH change in NHE3 expressed IRBIT KO MEF cells (Fig. 5 *A* and *B* and Fig. S6 *C* and *D*). He et al. reported that the phosphorylation of IRBIT and formation of a macrocomplex with NHE3, NHERF1, ezrin, and IRBIT contributes to insulin-dependent NHE3 activation (9, 10). Therefore, the phosphorylation state of IRBIT and the coexistence of endogenous regulatory factors or Long-IRBIT splice variants are responsible for the discrepancy between our results in IRBIT KO MEF cells and those of previous studies.

Recently, Yamaguchi et al. reported that AHCYL2 changes the apparent $Mg^{2+}$ affinity of NBCe1-B in bovine parotid acinar cells under $HCO^3$-deficient cellular conditions (22). However, Park et al. reported that the expression of LongV2 activated NBCe1-B in the same manner as IRBIT in HeLa cells (23). In this study, LongV2 has a tendency to slightly increase NBCe1-C activity, but no significant difference in IRBIT KO MEF cells was observed (Fig. 5 *C* and *D*), and it did not activate NBCe1-B in *Xenopus* oocytes (Fig. 6*D*). LongV2 mutant-deleted N-terminal 139 and 157 aa significantly activated NBCe1-B compared with full-length LongV2 (Fig. 6*D*). It was previously reported that the N-terminal truncated IRBIT was found as part of IRBIT expressed in COS-1 cells (cleavage site is described in Fig. 6*A* and Fig. S6*G*) (24). Therefore, it may be possible that N-terminal cleavage of LongV2 by endogenous proteases convert LongV2 to its active form for NBCe1 activity. In addition, multimer formation of LongV2 with the endogenous IRBIT family are responsible for the discrepancy between the results in IRBIT KO MEF cells, *Xenopus* oocytes, bovine parotid acinar cells, and HeLa cells. Additional studies using various types of cells and a combination of IRBIT family proteins, target molecules, and other cofactors may help us to reveal precise regulatory mechanisms in each physiological condition.

The Long-IRBIT splicing site corresponds to a consensus protein phosphatase-1 (PP1) docking site [K/R]-$X_{0-1}$-[I/V]-|P|-F (where |P| denotes any residue except proline). A number of glutamine residues (*Q*) in this site differ in each Long-IRBIT (Fig. 1*A* and Fig. S1 *B* and *C*) (LongV1: $Q = 1$, LongV2: $Q = 0$, LongV3a: $Q = 1$, LongV3b: $Q = 2$, LongV3c: $Q = 1$, LongV4: $Q = 0$). It is notable that the first lysine (K) for the consensus PP1 docking sequence is not included in LongV4. It was reported that the mutation of

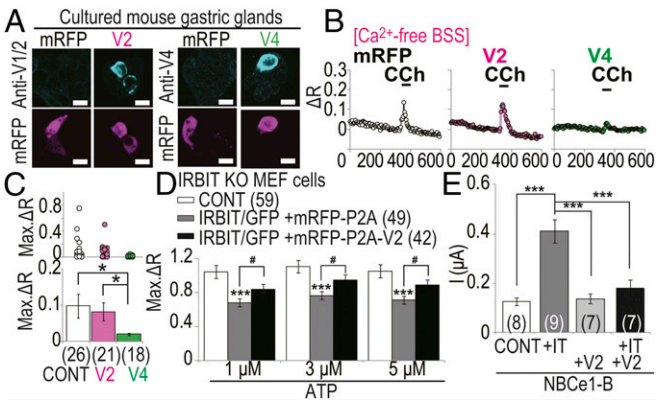


**Fig. 7.** LongV4 inhibited CCh-induced $Ca^{2+}$ release in gastric glands and LongV2 coexpression effected the regulation of $IP_3R$ and NBCe1-B by IRBIT. mRFP, mRFP-P2A; V2, mRFP–P2A-LongV2; V4, mRFP-P2A-LongV4. (*A*) Cultured gastric glands were transfected and stained with anti-LongV1/2 or anti-LongV4 Abs. (Scale bars, 10 μm.) (*B*) Representative $Ca^{2+}$ imaging of transfected gastric glands. CCh: 100 μM. (*C*) Quantitation of $Ca^{2+}$ peak amplitude (Max. ΔR). (*Upper*) Max. ΔR of each cell. (*Lower*) Average of Max. ΔR. The total cell numbers were indicated in each graph. *$P < 0.05$. (*D*) Peak amplitude (Max. ΔR) of ATP-induced $Ca^{2+}$ release activity in transfected IRBIT KO MEF cells. The total cell numbers were indicated in each graph legend. ***$P < 0.001$ compared with control cells, #$P < 0.05$. (*E*) NBCe1-B mediated currents at a holding potential −25 mV in *Xenopus* oocyte. The total cell numbers were indicated in each graph. ***$P < 0.001$.

IRBIT at the PP1 docking site affected the binding affinity of $IP_3R1$ (25). The PP1 docking site is located near the multiple phosphorylation sites of the IRBIT family. Therefore, it is possible that the number of glutamine residues in the Long-IRBIT splicing site affects the binding affinity for PP1 and the subsequent phosphorylation states of Long-IRBIT splice variants. It was reported that the phosphorylation state of IRBIT contributes to the binding to target molecules (3, 4, 7, 10, 13, 15). Therefore, the number of glutamine residues in the Long-IRBIT splicing site may determine the binding affinity of Long-IRBIT to target molecules.

In this study, we showed that the IRBIT family exhibits different binding affinities selectively conducive to several target pathways (Figs. 3–5). However, these data represent the mainly molecular property of homomultimer constructed by IRBIT or each Long-IRBIT splice variant. IRBIT and Long-IRBIT splicing variants form heteromultimers (Fig. 2 *A*–*D*), and LongV2 coexpression with IRBIT attenuates the effect of IRBIT (Fig. 7 *D* and *E*), indicating that the multimer formation alters target selectivity. Therefore, the combination of IRBIT family proteins may indicate functional diversity to regulate various target pathways in cells expressing multiple IRBIT family proteins. However, the results of LongV2 coexpression with IRBIT include the effect of homo- and heteromultimers. Therefore, additional studies using purified proteins composed of fixed combinations may help to reveal the detailed molecular properties of IRBIT family proteins and their target specificity.

IRBIT family proteins have diverse N-terminal regions and conserved serine-rich and C-terminal regions. All N-terminal regions of Long-IRBIT splice variants were structurally disordered, similar to IRBIT; therefore, the N-terminal regions of all IRBIT family proteins interact with various proteins. The conserved serine-rich region of IRBIT family proteins was modified by multiple phosphorylation events, and the C-terminal region forms homo- and heteromultimers of IRBIT family proteins. Therefore, N-terminal structural disorder, multiple phosphorylation events, and the combination of multimer formation serve as a base for the functional diversity of IRBIT family proteins as hub proteins, and contribute to calcium signaling, electrolyte transport, mRNA processing, cell cycle, apoptosis, and the regulation of catecholamine homeostasis through their interaction with multiple targets.

## Materials and Methods

A detailed documentation of the materials and methods can be found in *SI Materials and Methods*. All animal experiments were conducted in accordance with the RIKEN guidelines for animal experiments. Every effort was made to minimize the number of animals used.

**ACKNOWLEDGMENTS.** We thank the RIKEN BSI Research Resources Center for help with DNA sequencing analysis, and the RIKEN BSI-Olympus Collaboration Center for technical support; all members of our laboratories, especially Dr. Chihiro Hisatsune and Dr. Takeyuki Sugawara for fruitful discussions, Mr. Akito Nagayoshi for DNA construction, and Dr. Akitoshi Miyamoto for technical support for imaging experiment; and Editage (www.editage.jp) for English language editing. This study was supported by Japan Society for the Promotion of Science Grant-in-Aid for Scientific Research S 25221002 (to K.M.), for Scientific Research C 16K07075 (to K.K.), and for Scientific Research C 16K07068 (to A.M.).

1. Dunker AK, Cortese MS, Romero P, Iakoucheva LM, Uversky VN (2005) Flexible nets. The roles of intrinsic disorder in protein interaction networks. *FEBS J* 272:5129–5148.
2. Albert R, Jeong H, Barabasi AL (2000) Error and attack tolerance of complex networks. *Nature* 406:378–382.
3. Ando H, et al. (2006) IRBIT suppresses IP3 receptor activity by competing with IP3 for the common binding site on the IP3 receptor. *Mol Cell* 22:795–806.
4. Shirakabe K, et al. (2006) IRBIT, an inositol 1,4,5-trisphosphate receptor-binding protein, specifically binds to and activates pancreas-type Na+/HCO3- cotransporter 1 (pNBC1). *Proc Natl Acad Sci USA* 103:9542–9547.
5. Lee SK, Boron WF, Parker MD (2011) Relief of autoinhibition of the electrogenic Na/HCO3 cotransporter NBCe1-B: Role of IRBIT versus amino-terminal truncation. *Am J Physiol Cell Physiol* 302(3):C518–C526.
6. Yang D, et al. (2009) IRBIT coordinates epithelial fluid and HCO3- secretion by stimulating the transporters pNBC1 and CFTR in the murine pancreatic duct. *J Clin Invest* 119:193–202.
7. Yang D, et al. (2011) IRBIT governs epithelial secretion in mice by antagonizing the WNK/SPAK kinase pathway. *J Clin Invest* 121:956–965.
8. Park S, et al. (2013) Irbit mediates synergy between ca(2+) and cAMP signaling pathways during epithelial transport in mice. *Gastroenterology* 145:232–241.
9. He P, et al. (2015) Restoration of Na+/H+ exchanger NHE3-containing macrocomplexes ameliorates diabetes-associated fluid loss. *J Clin Invest* 125:3519–3531.
10. He P, Klein J, Yun CC (2010) Activation of Na+/H+ exchanger NHE3 by angiotensin II is mediated by inositol 1,4,5-triphosphate (IP3) receptor-binding protein released with IP3 (IRBIT) and Ca2+/calmodulin-dependent protein kinase II. *J Biol Chem* 285:27869–27878.
11. He P, Zhang H, Yun CC (2008) IRBIT, inositol 1,4,5-triphosphate (IP3) receptor-binding protein released with IP3, binds Na+/H+ exchanger NHE3 and activates NHE3 activity in response to calcium. *J Biol Chem* 283:33544–33553.
12. Tran TM, et al. (2013) IRBIT plays an important role in NHE3-mediated pHi regulation in HSG cells. *Biochem Biophys Res Commun* 437:18–22.
13. Kiefer H, et al. (2009) Inositol 1,4,5-triphosphate receptor-binding protein released with inositol 1,4,5-triphosphate (IRBIT) associates with components of the mRNA 3′ processing machinery in a phosphorylation-dependent manner and inhibits polyadenylation. *J Biol Chem* 284:10694–10705.
14. Arnaoutov A, Dasso M (2014) Enzyme regulation. IRBIT is a novel regulator of ribonucleotide reductase in higher eukaryotes. *Science* 345:1512–1515.
15. Ando H, et al. (2015) IRBIT interacts with the catalytic core of phosphatidylinositol phosphate kinase type Iα and IIα through conserved catalytic aspartate residues. *PLoS One* 10:e0141569.
16. Bonneau B, et al. (2016) IRBIT controls apoptosis by interacting with the Bcl-2 homolog, Bcl2l10, and by promoting ER-mitochondria contact. *eLife* 5:e19896.
17. Kawaai K, et al. (2015) IRBIT regulates CaMKIIα activity and contributes to catecholamine homeostasis through tyrosine hydroxylase phosphorylation. *Proc Natl Acad Sci USA* 112:5515–5520.
18. Ando H, Mizutani A, Mikoshiba K (2009) An IRBIT homologue lacks binding activity to inositol 1,4,5-trisphosphate receptor due to the unique N-terminal appendage. *J Neurochem* 109:539–550.
19. Xue B, Dunbrack RL, Williams RW, Dunker AK, Uversky VN (2010) PONDR-FIT: A meta-predictor of intrinsically disordered amino acids. *Biochim Biophys Acta* 1804:996–1010.
20. Ando H, Mizutani A, Matsu-ura T, Mikoshiba K (2003) IRBIT, a novel inositol 1,4,5-trisphosphate (IP3) receptor-binding protein, is released from the IP3 receptor upon IP3 binding to the receptor. *J Biol Chem* 278:10602–10612.
21. Schwark JR, et al. (1998) S3226, a novel inhibitor of Na+/H+ exchanger subtype 3 in various cell types. *Pflugers Arch* 436:797–800.
22. Yamaguchi S, Ishikawa T (2014) AHCYL2 (long-IRBIT) as a potential regulator of the electrogenic Na(+)-HCO3(-) cotransporter NBCe1-B. *FEBS Lett* 588:672–677.
23. Park PW, Ahn JY, Yang D (2016) Ahcyl2 upregulates NBCe1-B via multiple serine residues of the PEST domain-mediated association. *Korean J Physiol Pharmacol* 20:433–440.
24. Devogelaere B, et al. (2006) Binding of IRBIT to the IP3 receptor: Determinants and functional effects. *Biochem Biophys Res Commun* 343:49–56.
25. Devogelaere B, et al. (2007) Protein phosphatase-1 is a novel regulator of the interaction between IRBIT and the inositol 1,4,5-trisphosphate receptor. *Biochem J* 407:303–311.
26. Kawaai K, et al. (2009) 80K-H interacts with inositol 1,4,5-trisphosphate (IP3) receptors and regulates IP3-induced calcium release activity. *J Biol Chem* 284:372–380.
27. Gliddon BL, Nguyen NV, Gunn PA, Gleeson PA, van Driel IR (2008) Isolation, culture and adenoviral transduction of parietal cells from mouse gastric mucosa. *Biomed Mater* 3:034117.
28. Muto Y, Nagao T, Yamada M, Mikoshiba K, Urushidani T (2001) A proposed mechanism for the potentiation of cAMP-mediated acid secretion by carbachol. *Am J Physiol Cell Physiol* 280:C155–C165.
29. Suzuki M, et al. (2010) Defective membrane expression of the Na(+)-HCO(3)(-) cotransporter NBCe1 is associated with familial migraine. *Proc Natl Acad Sci USA* 107:15963–15968.
30. Anderson CM, Thwaites DT (2007) Regulation of intestinal hPepT1 (SLC15A1) activity by phosphodiesterase inhibitors is via inhibition of NHE3 (SLC9A3). *Biochim Biophys Acta* 1768:1822–1829.
31. Krishnan D, et al. (2015) Carbonic anhydrase II binds to and increases the activity of the epithelial sodium-proton exchanger, NHE3. *Am J Physiol Renal Physiol* 309:F383–F392.
32. Yamazaki O, et al. (2011) Functional characterization of nonsynonymous single nucleotide polymorphisms in the electrogenic Na+-HCO3- cotransporter NBCe1A. *Pflugers Arch* 461:249–259.
33. Satoh N, et al. (2016) A pure chloride channel mutant of CLC-5 causes Dent's disease via insufficient V-ATPase activation. *Pflugers Arch* 468:1183–1196.
34. Gomi T, et al. (2008) Cloning, bacterial expression, and unique structure of adenosylhomocysteine hydrolase-like protein 1, or inositol 1,4,5-triphosphate receptor-binding protein from mouse kidney. *Biochim Biophys Acta* 1784:1786–1794.